Myosin VI undergoes a 180° power stroke implying an uncoupling of the front lever arm

Jeff G. Reifenberger[a,1], Erdal Toprak[b,1], HyeongJun Kim[a], Dan Safer[c], H. Lee Sweeney[c,d,2], and Paul R. Selvin[a,b,3]

[a]Department of Physics, University of Illinois, Urbana, IL 61801; [c]Department of Physiology and [d]Pennsylvania Muscle Institute, University of Pennsylvania School of Medicine, 3700 Hamilton Walk, Philadelphia, PA 19104-6085; and [b]Center for Biophysics and Computational Biology, University of Illinois, Urbana, IL 61801

Edited by Edwin W. Taylor, Northwestern University Feinberg School of Medicine, Chicago, IL, and approved September 3, 2009 (received for review January 3, 2009)

We simultaneously measure both the step size, via FIONA, and the 3-D orientation, via DOPI, of the light-chain domain of individual dimeric myosin VIs. This allows for the correlation of the change in orientation of the light chain domain to the stepping of the motor. Three different pairs of positions were tested using a rigid bifunctional rhodamine on the calmodulin of the IQ domain. The data for all three labeling positions support the model that the light chain domain undergoes a significant rotation of approximately 180°. Contrary to an earlier study [Sun, Y. et al. (2007) *Mol Cell* 28, 954–964], our data does *not* support a model of multiple angles of the lever arm of the lead head, nor "wiggly" walking on actin. Instead, we propose that for the two heads of myosin VI to coordinate their processive movement, the lever arm of the lead head must be uncoupled from the converter until the rear head detaches. More specifically, intramolecular strain causes the myosin VI lever arm of the lead head to uncouple from the motor domain, allowing the motor domain to go through its product-release (phosphate and ADP) steps at an unstrained rate. The lever arm of the lead head rebinds to the motor and attains a rigor conformation when the rear head detaches. By coupling the orientation and position information with previously described kinetics, this allows us to explain how myosin VI coordinates its heads processively while maintaining the ability to move under load with a (semi-) rigid lever arm.

FIONA | fluorescence | motility | single molecule assay | unconventional myosin

Despite fairly intensive study, how myosin VI moves remains elusive. It is known that myosin VI moves toward the minus end of actin in contrast to all other myosins (1). Myosin VI also has a large and variable step size of ≈30 ± 12 nm with occasional back steps of approximately 13 ± 8 nm (2, 3), which is made possible by a combination of a short calmodulin-containing lever arm (4) and a lever-arm extension that is created by the unfolding of a three-helix bundle (5). The processive stepping is a hand-over-hand motion (6, 7) and has recently been reported to involve a "wiggly" movement around actin (8). This is in contrast to myosin V, arguably the best understood myosin motor (9), which takes a 36-nm step size (10), in a hand-over-hand fashion (11), tilting its large lever arm approximately 70° (12, 13), in a relatively straight fashion, with some twisting about the actin axis (13–15).

The atomic structure of myosin VI has been revealed in the post-power stroke states (16) and a truncated form in the pre-power stroke states (17). It is largely the same as myosin V, but myosin VI has two inserts, one near the nucleotide pocket, which allows it to fine-tune its response to ADP and ATP, and a second unique insert at the end of the converter domain, where the lever arm connects to the motor domain, which repositions the lever arm and reverses the power stroke (18, 19).

While it is unclear as to the exact degree of rotation that the power stroke undergoes, it is undoubtedly large. Ménétrey et al., based on the crystal structures, suggested it was nearly 180° (16, 17). Bryant et al., based on a series of single-headed constructs in an optical trap, also concluded that the lever arm undergoes a 180° redirection during the power stroke (20). Sun et al., based on single-molecule fluorescence angular changes, stated that their data were most consistent with variable lever arm positions, with the majority involving an approximate 180° reorientation of the lever arm (8). Furthermore, they observed "chaotic left-right wiggling" of the lever arm as the myosin VI moves along the actin filament.

The aspect of the myosin VI processive mechanism that had been most difficult to reconcile is how, like myosin V (21), myosin VI gates, or stalls, its lead head in a strongly bound actin state until the rear head has detached from actin. In the case of myosin V, the lever arm of the lead head cannot complete its swing due to intramolecular strain, and thus ADP release from the lead head is greatly slowed (21). While this is slowed down, ADP can rapidly dissociate from the rear head, allowing ATP to rapidly bind and dissociate the rear head from actin and leading to forward stepping. This has been directly observed by visualizing an approximate 70° swing of the lever arm (12, 13) of a stepping myosin V dimer. In contrast with myosin V, the lead head of a myosin VI dimer walking on actin releases ADP at a rate that is the same as in the absence of strain; i.e., it is strain independent (18). Instead of slowing down ADP release, gating of the lead head in myosin VI is accomplished by preventing rapid binding of ATP (18).

One confusing issue that is ongoing has to do with the highly variable step size of myosin VI. Sun et al. (8), found that the orientation of myosin VI's lever arm varies in orientation, with the lead head having a different and variable orientation than the rear head (presumably due to a lever arm that did not always undergo a 180° swing). It is possible that this corresponds to the variable translational steps taken by myosin VI. However, their technique did not allow for simultaneous resolution of lever arm angle and step size, making the connection tenuous.

To shed light on myosin VI's walking mechanism, we measured simultaneously the step size via fluorescence imaging with one-nanometer accuracy (FIONA) and angular changes via defocused orientation and position imaging (DOPI) of the light chain. The major advantage over previous fluorescence measurements is the ability to simultaneously measure the translational step size and the lever arm's angular change. This is similar, although slightly different from (see *Materials and Methods* and *SI Text*), to what we did with myosin V (13). We find that the lever arm of the double-headed myosin VI indeed takes a 180° swing toward the minus end of actin, but contrary to the results of Sun et al., our data does *not* support a model of multiple angles of the lever arm of the lead head.

Author contributions: J.G.R., E.T., H.L.S., and P.R.S. designed research; J.G.R., E.T., and D.S. performed research; J.G.R. and E.T. contributed new reagents/analytic tools; J.G.R., E.T., and H.L.S. analyzed data; and J.G.R., E.T., H.K., H.L.S., and P.R.S. wrote the paper.

The authors declare no conflict of interest.

This article is a PNAS Direct Submission.

[1]J.G.R. and E.T. contributed equally to this work.

[2]To whom correspondence may be addressed at: Department of Physiology, University of Pennsylvania., B400 Richards Bldg., 3700 Hamilton Walk, Philadelphia, PA 19104-6016. E-mail: lsweeney@mail.med.upenn.edu.

[3]To whom correspondence may be addressed at: Physics Department, 1110 West Green Street, Loomis Laboratory, University of Illinois, Urbana, IL 61801. E-mail: selvin@uiuc.edu.

This article contains supporting information online at www.pnas.org/cgi/content/full/0900005106/DCSupplemental.

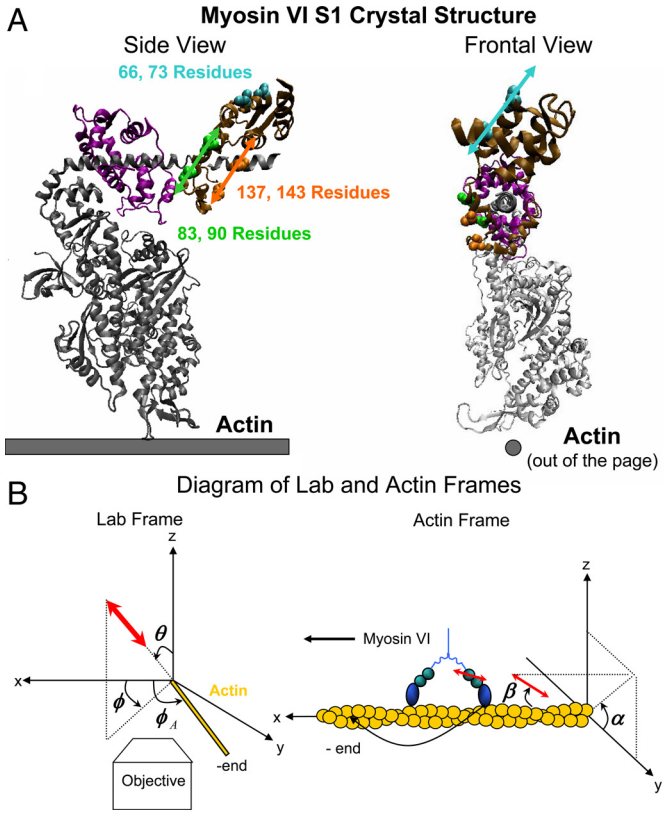

Fig. 1. Labeling and orientation of Myosin VI. (*A*) Myosin VI rigor-like (absence of nucleotide) crystal structure from (16) in two different orientations demonstrating the three pairs of locations that were labeled with a bifunctional rhodamine for the experiment. Green highlights the 83, 90 residues, orange the 137, 143 residues, and cyan the 66, 73 residues that were labeled. The location of actin for both orientations is shown in gray for reference. (*B*) A diagram of the lab frame angles (θ, ϕ) and the actin frame (α, β).

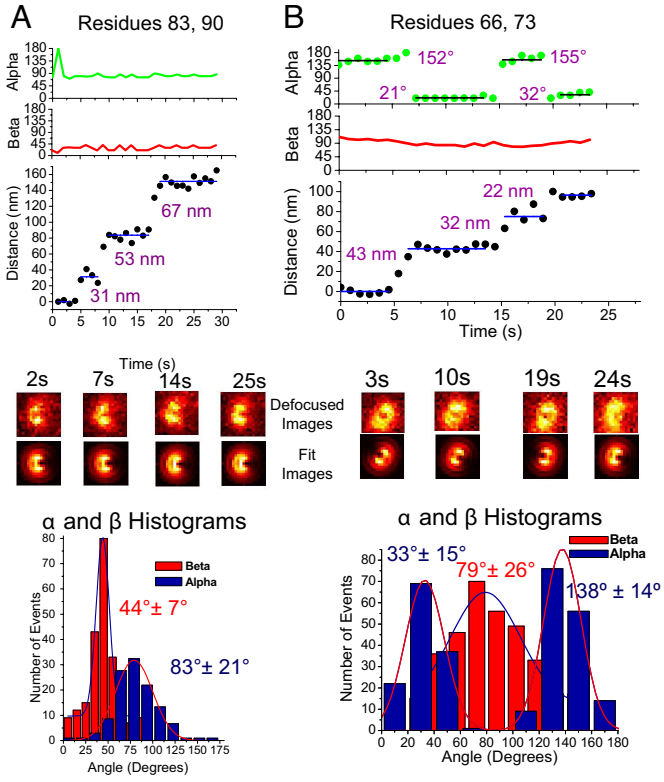

Fig. 2. Individual traces of myosin VI labeled at the (*A*) [83, 90] position and the (*B*) [66, 73] position. The values of α and β remain constant at [83, 90], and α alternates between two values while β remains constant for [66, 73]. In both cases, the motor walks approximately 100 nm during the trace. The defocused images and the histograms are also shown below. All values in histogram are averaged over the dwell time of an individual myosin VI molecule. All histograms fit to a single Gaussian.

Our results are best explained by an uncoupling of the lever arm from the converter during the initial product release steps by the lead head on actin.

Results

Sun et al. recently published a paper suggesting that the step size of myosin VI determined the orientation between the leading and trailing lever arms of the motor. However, the experimental technique used by Sun et al. was only able to measure the angles of the lever arm and hence unable to correlate any measured angular changes with positional changes (i.e., movement) of the motor. To correlate the stepping of the motor with angular changes, an improved method for measuring the step size via FIONA and the 3-D orientation via DOPI was developed. In this method, the focused (FIONA) and out-of-focused (DOPI) information were acquired simultaneously. This is an improvement on a previous paper where previously they were taken serially (13). (Fig. S1).

Three pairs of amino acids on the calmodulin were mutated to cysteines based on the crystal structure of the rigor state myosin VI. These were labeled with a bifunctional rhodamine (Fig. 1*A*) (16). The first pair was at the 83rd and 90th residues (highlighted green), second pair at the 137th and 143rd residues (highlighted orange), and finally the third pair at the 66th and 73rd residues (highlighted blue). The calmodulins were then exchanged onto myosin VI, using care that only the calmodulin on the second IQ was exchanged (see *Materials and Methods*). The line drawn in Fig. 1*A* between each pair of residues shows the approximate orientation of the dipole moment of the bifunctional probe and hence the orientation of the probe. The gray line shows the actin orientation. The light chain domain, i.e., the lever arm, of myosin VI and actin can be thought of as forming a plane in which the dipole moment of the bifunction rhodamine for the [83, 90] and the [137, 143] labeled positions are parallel to the LCD-actin plane. The dipole moment of the [66, 73] labeled position is at a slight angle to the LCD-actin plane. This can be seen on the right hand side of Fig. 1*A*. The orientation of the dipole moment of the bifunction rhodamine to the LCD-actin plane plays an important role in understanding the de-focused data presented later.

Actin was immobilized on a coverslip with biotin-streptavidin linkers, and myosin VI was added to a flow cell containing actin and 10–20 μM ATP. At this low concentration of ATP, single steps with significantly long dwell times were observable. An oxygen scavenger was used to extend the lifetime of the bifunctional rhodamine and movies were taken with exposure times between 0.5 and 1.0 s (11). Fig. 1*B* shows the lab frame with actin oriented an angle θ_A in the x-y plane (i.e., on the glass surface). The two angles of the probe in the lab frame θ and ϕ are measured and then transferred to the more relevant actin frame coordinates of α and β.

Ninety-one myosin VI molecules were measured for the [83, 90] labeling position, 53 molecules were measured for the [137, 143] labeling position, and 30 molecules were measured for the [66, 73] labeling position. Fig. 2 *A* and *B* show an individual trace of a single myosin VI molecule walking along actin for the [83, 90] and for the [63, 73] labeling positions respectively. The trace for [137, 143] is very similar to [83, 90] and shown in Fig. S2. The defocused patterns coupled with the position information shown

in Fig. 2*A* indicate the orientation of the LCD, both α and β, remains unchanged as myosin VI walks along actin. This is in contrast to myosin V, where the β angle changes from 57–128° (12, 13) and the azimuthal angle, α, remains unchanged as the motor moves processively along actin. To further demonstrate that during its motion along actin myosin VI's two angles remain constant, a histogram of the change in α and β for each step (data not shown) can be fit by a single Gaussian. The fit for the change in α is $0 \pm 16°$ while the fit for the change in β is $1 \pm 10°$. In these fits, the distribution of the change in α is slightly broader than that of β. It was observed that on rare occasions after remaining at a constant azimuthal angle for several steps that an individual myosin VI motor's α angle would suddenly change to a new value after a step, but then remain at the new orientation during subsequent steps along actin.

Fig. 2*A Lower* shows the α and β histograms of the averaged values within a single dwell period for the [83, 90] labeling position, with both histograms fit by a single Gaussian. The fit to the histogram of the α distribution yielded the following value $83 \pm 21°$ and for β it was $44 \pm 7°$. (For position [137, 143], the α distribution is $73 \pm 15°$ and the β distribution is $46 \pm 9°$, see Fig. S2.) One can clearly see for both the [83, 90] and the [137, 143] labeled positions on the calmodulin that the defocused pattern does not change as myosin VI walks along actin, but rather remains at a constant value. The fact that the two labeling positions, [83, 90] and [137, 143], yield the same orientation in α and β is not an unexpected result since the probes are nearly parallel to each other based on the crystal structure shown in Fig. 1*A*. (Movie S1 shows both the focused and defocused images of myosin VI labeled at the [83, 90] position as it walks along actin.)

The results for myosin VI labeled at the [66, 73] position on calmodulin are slightly more complicated than for the other two positions (Fig. 2*B*). The top half of Fig. 2*B* is an individual trace of a single myosin VI protein. In the trace, the alpha angle flips between approximately 155 and 25° while the beta angle remains constant for each step. In the bottom half of Fig. 2*B*, a histogram of the α and β values within the dwell time of all myosin VI motors labeled at the [66, 73] position is shown. Two Gaussians fit to the α histogram yields two values of $33 \pm 15°$ and $138 \pm 14°$, and a single Gaussian fit to the β histogram with a value of $69 \pm 20°$.

Finally, the data on the step size and stepping kinetics for all labeled sites match those of previously reported values (6, 7). The plots are shown in Fig. S3. The average step sizes toward the minus end of actin were 50 ± 25 nm, and toward the plus end of actin were 31 ± 13 nm. (See *SI Text*, Use of the Dual View, for further discussion on step size and distance resolution.)

Discussion

Myosin VI undergoes a 180° Rotation of Light-Chain Region. Before discussing the details of myosin VI data, it is important to keep the previous defocused imaging measurements on myosin V in context when thinking about what might be expected for myosin VI. In the case of myosin V, when the orientation of the lever arm was measured via defocused imaging, the β angle of the trailing head was 57° and when the head was leading it was 128°: hence, the change in β was approximately 71° (13). As demonstrated in Fig. 3*A*, if myosin VI walks in a hand-over-hand method through a rotation of its light chain domain (i.e., the lever arm) similar to myosin V, then one would expect the bifunctional probe to alternate between one β angle for the post-power stroke state (the trailing head) and a second β angle for the pre-power stroke state (the leading head). For example, the rotation shown in Fig. 3*A* would result in a rotation of the LCD of myosin VI during the power stroke that is near $\Delta\beta = 70°$. If the lever arm rotates as shown, then one would expect to see a rotation of 90–100° in the ϕ angle within the lab frame while the θ angle will remain fairly constant. However, no such rotation in β is observed for all three labeled positions on the calmodulin.

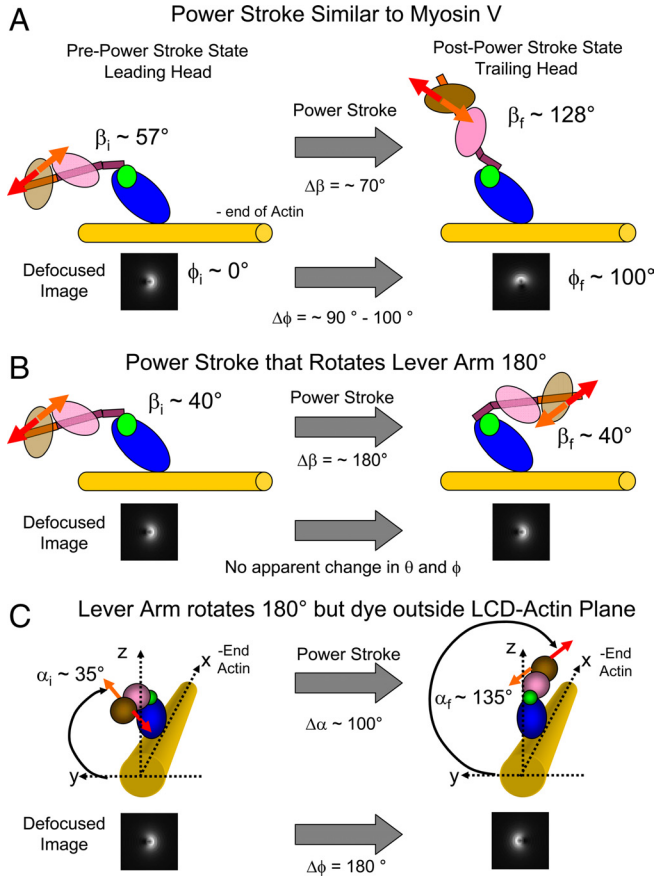

Fig. 3. Defocused images for various models of myosin VI motion. (*A*) The expected defocused images if myosin VI's LCD rotates through an angle similar to myosin V during the power stroke. (*B*) Expected defocused images if the LCD of myosin VI rotates 180° when the dye is within the plane created by the LCD and actin. (*C*) Expected defocused images if the dye is not within the plane created by the LCD and actin if the lever arm rotates 180°.

While at first glance the data for all three labeled positions might seem contradictory, the explanation that best fits the data are that the light chain of myosin VI undergoes a 180° rotation with each step. The first evidence for a 180° rotation is from the observation that the β angle for all three labeled positions on the calmodulin remains constant throughout the motion of myosin VI. Fig. 3*B* demonstrates how a 180° rotation will result in no change in the measured value of the β angle for the [83, 90] and [137, 143] labeled calmodulin positions, although the plot is also applicable to the β angle of the [66, 73] position. The dipole of the fluorophore is shown with the orange/red arrow on the left hand side of Fig. 3*B* in the pre-power stroke state. In this state the red arrow is pointing down. As the lever arm rotates during the power stroke the dipole rotates 180° so that the red arrow is now facing up (right hand side of Fig. 3*B*). While the red and orange arrows flip position during the power stroke, the emission pattern from a dipole is degenerate when rotated by 180° so that the defocused pattern would remain unchanged. That is exactly what is observed for the [83, 90] and [137, 143] labeled calmodulin positions. Since the dipoles of these two positions are parallel to the plane formed by the light chain domain (i.e., where the calmodulins bind) of myosin VI and the actin filament the defocused pattern remains unchanged as myosin VI walks along actin resulting in the α and β angles remaining unchanged as well.

While the [66, 73] labeled position on the calmodulin is slightly more complicated, the β angle remained unchanged as well during myosin VI motion again supportive of a 180° rotation of the light

chain domain. However, the [66, 73] labeled position of calmodulin yields even further evidence supportive of a 180° rotation than the [83, 90] and [137, 143] labeled positions. Fig. 2*B* showed that while β remains constant, α changed with each step of myosin VI. Fig. 3*C* demonstrates how this is further evidence of a 180° rotation of the light chain domain. Unlike the other two labeled calmodulin positions, the [66, 73] position resulted in the dipole not being parallel to the plane formed by the light chain domain and the actin filament. This results in the dipole having a different azimuthal angle, α, as the light chain rotates during the power stroke. This is measured in the lab frame through a rotation in ϕ of 180°. This was what was observed in Fig. 2*B*.

Finally, why did the α angles for the [83, 90] and [137, 143] labeled positions rarely change as myosin VI walked along actin? Since the dipole of these two positions is in the same plane as the light chain domain and actin filament we would expect the α angle to remain unchanged during the 180° power stroke of the lever arm. However, since myosin VI takes such a broad distribution of step sizes as shown in Fig. S3, then eventually the α angle of the probe should change as the myosin VI binds to different actin monomers with different azimuthal angles. Yet, the data does not support an *individual* myosin VI binding to actin monomers with significantly different azimuthal angles and hence the motor does not appear to rotate around the actin filament as it walks. Rather it appears that myosin VI walks in a relatively straight line along actin thereby keeping a relatively constant α angle. Remember that the broad distribution of step sizes in Fig. S3 is a result of many myosin VI molecules and not a single molecule. Hence it is plausible that an individual molecule will only access the actin monomers directly in front of the motor and rarely attempt to bind to monomers that would require a significant rotation of the head around the actin. However, we cannot rule out the fact that the experimental setup played a role in our observations of no change in α for the [83, 90] and [137, 143] labeled calmodulin positions. The α angle for both labeled positions is centered near the top of the actin filament. This is most likely a result of the actin being attached to the glass surface and myosin VI only having access to the top half of the filament due to steric constraints from the surface, thereby preventing or at least reducing the likelihood of myosin VI rotating around actin as it walks along the filament.

Our results do not support a small rotation of the lever arm of myosin VI as it walks along actin as was seen for myosin V but a large rotation of nearly 180°. While Sun et al. did support our results of a 180° rotation of the lever arm of myosin VI (8), our work differs from Sun et al. in that we never saw differing β angles for different step sizes of myosin VI for all three labeled positions on the calmodulin. It is hard to imagine how a 180° rotation would result in different β angles for the light chain domain of an emitting dipole due to the degeneracy of the dipole emission. However, because Sun et al. collected data on a much faster time frame, approximately 10-fold faster than our work, it cannot be ruled out that they observed the lever arm in some unsettled position while we measured the lever arm in its final resting position.

Uncoupling of the Lever Arm. The properties of myosin VI during processive movement have been difficult to explain, and all likely emanate from the fact that it is a reverse direction myosin that must coordinate, or gate, its heads to allow both processive movement and anchoring (22, 23). Myosin VI was found to have an irregular, but large, step-size (2), and achieved this using an unusual extension of the lever arm (5, 24). However, this lever arm extension of myosin VI is largely alpha-helical (5) and cannot be so compliant as to allow the lead head to release its hydrolysis products, bind ATP and detach from actin while the rear head is attached (i.e., no "gating" of the lead head) in a processive dimer (18). Furthermore, if the lever arm extension was too compliant, we might not see a change in the lever arm angle. The lever arm of the lead head would rapidly approach its rigor or ADP-bound positions since phosphate release, which limits the rate of transition out of the pre-power stroke conformation, occurs at approximately 70 s^{-1}. This rate is much faster than the imaging time of our experiment (18). [Note that based on cryo-EM, the rigor and ADP positions of the lever arm are similar (1).] This view is inconsistent with the data in Fig. 2*B*, in which the α angle is observed to change with each step, which is consistent with a 180° lever arm swing when the myosin VI lead head becomes a rear head (i.e., during stepping).

A recent paper by Sun et al. (8) proposed that myosin VI walked on actin with large and variable tilting of the LCD. Our data shows no such variability in tilting of the LCD of myosin VI. One possible explanation, as mentioned earlier, of the inconsistency between our results and their results is the approximate 10-fold better time resolution of their technique. However, our traces showed clear stepwise movements confirming that our time resolution was adequate to capture steps and lever arm reorientations at the low ATP concentrations (10 μM) that we used. Furthermore, being able to accurately track myosin VI's movements along both longitudinal and transversal axis of the actin filaments allowed us to perform an extra analysis step to examine the suggested "wiggly" movement of myosin VI. Here we measured the side-to-side distances of the bifunctional rhodamine probes from the actin axis (Fig. S4). Overall, the average distance from the actin axis was approximately 0 nm. However, if the lever arm of myosin VI was going through a wiggly movement as described by Sun et al., the distance of the probe from the actin axis would fluctuate between approximately −5 and +5 nm. Hence, our result provides evidence against the suggested model by Sun et al.

Sun et al. also saw a difference between the β angle for the forward and trailing head of myosin VI. We saw no evidence of a change in β as myosin VI walks along actin for all three of the labeled positions, which, again, is most consistent with a rotation of the lever arm through 180°. While Sun et al. also claim a 180° rotation is most consistent with their data, they further state that the distance between the trailing head and the leading head can affect the orientation of the leading head's lever arm and hence this is why they see two distributions in β. The most likely explanation for the apparent inconsistencies between our work and their work is a difference in data analysis.

Sun et al., because they did not have access to translational data, chose an artificial (wrong) choice. In our case, we consistently chose the dipole angle to be in the upper hemisphere ($0 \leq \alpha \leq 180°$; $0 \leq \beta \leq 180°$), which was set by the angles that were measured in the lab frame. On the other hand, Sun et al. chose a hemisphere that lies in between the two hemispheres (i.e., $-60° \leq \alpha \leq 120°$; $0 \leq \beta \leq 180°$), which imposes a considerable ambiguity on their analysis. In our experiments, where we used the same CaM labeling as they did (Cys-66–73), the β values did not change and the average value for β was approximately 70 ± 15°. The α values alternated between 33 ± 15° and 152 ± 15°. If we choose the same hemisphere as Sun et al. did, our angular values would alternate between ($\alpha = 33°$, $\beta = 70°$) and ($\alpha = -28°$, $\beta = 110°$), which are very similar to the values reported by Sun et al. (see Fig. S5). The advantage of our imaging technique is that we can correlate translational movement with any change in the LCD's angle. Again, for the time scale of our images, we simply do not see a change in the value of β as myosin VI moves.

Ultimately, the gating of the heads of myosin VI must be different from that of any other processive, plus end-directed, myosins (18). With myosin V, the gating of the heads is largely due to the intramolecular strain, which prevents the lead head from rotating its converter into a position that allows the active site to release MgADP (21). This traps the lever arm of the lead head of myosin V in a position that has a marked angular change as compared with the rear head, which has rotated sufficiently to release all products and can rapidly rebind MgATP (13). For myosin VI, the situation has to be different, since the vector of the intramolecular strain felt by the lead and rear heads is reversed. If the converter subdomain of the lead head of myosin VI was prevented from rotating, then it

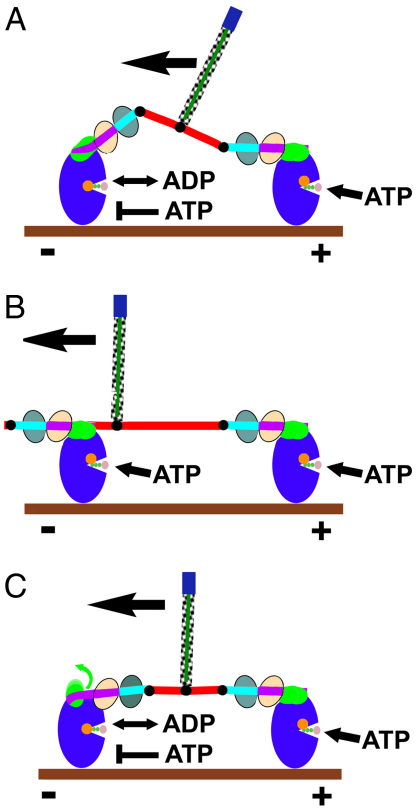

Fig. 4. Myosin VI movement on actin. (*A*) Expected result. The lead head maintains coupling of insert 2 (purple) to the converter subdomain (green) and lever arm (the first oval represents the insert 2-bound CaM, and the second oval represents the IQ-bound CaM, where the probes reside) rotates until internal strain prevents further rotation (until trailing head is detached by ATP binding). This was the expected result, but is ruled out due to the lack of any change in β angles of the probes. In particular, the change in β in this figure is clearly not 180°, as was seen in all three labeled positions. Note: double-headed arrow indicates that nucleotide is going in and out freely (ADP); single-headed arrow indicates rapid and nearly irreversible binding (ATP with arrow); no arrow indicates the nucleotide is blocked (ATP). (*B*) Both heads are in same conformation. The lever arm extension (red) is highly extensible, so the lead head can undergo rotation into the same conformation as the trailing head. This is ruled out by two separate lines of evidence. Although none of the probes detect a β change, the 66–73 CaM probe detects a change in the α angle between the two heads (Figs. 2 and 3), demonstrating that they are not in identical conformations. Additionally, in the absence of any internal strain, the lead head would be able to rebind ATP, destroying processive movement (see 18). We note that this model is consistent with a 0° change in the lever arm, but is not consistent with a 180° change in the lever arm, which is what is seen with [66, 73]. (*C*) Hypothetical model consistent with all data. In order to release ADP rapidly (as is observed; ref. 18), there must be some rotation of the converter (green) subdomain of the lead head (indicated by green arrow) to allow the nucleotide binding elements to alter their conformation. This rotation should increase the intramolecular strain. However, there is not a corresponding tilting of the lever arm in our experiment, which would be expected if it remained bound to the converter. Therefore, we propose that, in the absence of strain, the lever are is weakly coupled to the pre-power stroke converter conformation. The intramolecular strain created upon binding of the lead head of a dimer leads to detachment (complete uncoupling) of insert 2 (purple) and the lever arm. Furthermore, as has been observed in kinetic experiments (18), ATP cannot rapidly bind to the lead head. Therefore, the intramolecular strain must prevent recoupling of the lever arm, which prevents the formation of a rigor-like conformation of the converter and motor (which would bind ATP at the unstrained rate). This could result in fluctuation of the converter conformation, and possibly fluctuation in the tethered lever arm position (but not beta angle) consistent with earlier observations of Yildiz et al. (26). The detached insert 2 would be held (by intramolecular strain) in a position approximately 180° from its rigor position (trailing head), consistent with the observed probe angles in this study. Upon detachment of the trailing head by ATP binding, insert 2 would recouple to the converter as it assumes its rigor-like conformation, becoming the new rear head. This is consistent with the 180° swing seen for all three positions. Also note that we indicate the approximate position of our leucine zipper as a solid blue cylinder at the end of our schematic of the myosin VI dimer. In order to account for the observed beta angles of the CaM-containing lever arms, we indicate a second point of dimerization immediately following the lever arm extension (red), as we have recently demonstrated (7).

could not release ADP. However, it has been shown that the lead head of a processive myosin VI dimer releases both phosphate and ADP at essentially the same rate as in the absence of strain (18). Instead of ADP release being blocked, the lead head is stalled on actin until the rear head detaches due to extremely slow binding of ATP (18). This implies that while the converter domain of the lead head can rotate sufficiently to release the hydrolysis products, intramolecular strain greatly slows the lead head from attaining a rigor conformation.

We are left with a paradox. There needs to be a mechanism to allow significant rotation of the converter subdomain of the lead head of myosin VI to allow product release, but it does not involve a highly compliant linkage between the heads (since we observe a 180° angular change). At the same time, our current experiments suggest that the lead head has its lever arm held at an angle similar to that seen in the crystal structure of the pre-power stroke ($ADP{\cdot}P_i$) state, even though it must be in a very different state to explain the product release kinetics.

A plausible explanation of our results is that in the pre-power stroke state in the absence of strain, the lever arm of myosin VI is only weakly associated with the converter. In a processive dimer, the development of intramolecular strain upon attachment of the lead head results in a complete uncoupling of the lever arm from the converter. This result allows the product release steps on actin to occur at a rate similar to the unstrained rate (18). Due to the intramolecular strain and the position of the rear head, the uncoupled lever arm of the lead head is held parallel to the actin filament in the states that allow product release. This is consistent with the structural data we have to date (16, 17). While the lever arm appears tightly coupled to the converter in the rigor-like state of myosin VI (16), the model of the lever arm position in the pre-power stroke state published by Ménétrey et al. (17) had very weak interactions between the converter and first calmodulin of the lever arm. Strain could break such interactions and allow the lever arm of the lead head to come free of the converter (see Fig. 4). This contrasts with the model of Sun et al. (8), which postulated that there is a significant compliance at the base of the lever arm to account for the variable lever arm angles that they observed. Furthermore, they ruled out the type of uncoupling that we are proposing based on the logic that the lever arm would be floppy, but we counter this argument with the notion that the intramolecular strain holds the lever arm parallel to the actin filament.

Furthermore, note that unlike other myosins that have been characterized, the converter of myosin VI is not found in a single conformation (17). There is a major rearrangement of the converter itself between the pre-power stroke and rigor states of the motor. What our new data suggests, consistent with the structures, is that the pre-power stroke conformation of the converter does not maintain a tight coupling of the lever arm, while the rigor conformation does. If one postulates that ATP can only bind rapidly to myosin VI once it achieves its rigor conformation, then this explains the paradox for myosin VI movement. The converter can rotate when the lever arm becomes free, releasing ADP at the unstrained rate, but the converter rotation is prevented from fully attaining its rigor conformation due to the composite stiffness of the linkage between the lever arm and the converter (which may be comprised of all or part of the helix immediately preceding the insert 2-CaM complex) and the unfolded three-helix bundles that constitute the extensions of the myosin VI lever arms (5).

Note our data and model argue against the model of myosin VI

recently proposed by Spink et al. (25). In this model, the CaM-containing lever arm of myosin VI is extended by long single alpha helices and dimerization between the myosin VI monomers occurs only in the region of their cargo binding domains (approximately the position of the GCN4 leucine zipper in our HMM construct). This would predict that there be a significant change in beta angle between the lead and rear heads, as shown in the proposed structure in their paper. Our data are consistent with a region of dimerization between two myosin VI monomers that immediately follows the lever arm extension, as was recently shown (5). This is indicated in the diagram of Fig. 4 and further discussed in the *SI Text*.

In summary, the orientation data for myosin VI coupled with the position data demonstrates that there is a 180° rotation during the power stroke, and not variable angles of rotation. Furthermore orientation/position data suggest that for the two heads to coordinate their processive movement that the lever arm of the lead head must be uncoupled from the converter until the rear head detaches.

Materials and Methods

Myosin VI Construct and Expression. As previously described (27), a ''zippered'' dimeric myosin VI construct was created by truncation of porcine myosin VI at Arg-994, which was followed by a leucine zipper (GCN4) to ensure dimerization, and FLAG tag for purification. This construct was used to create a recombinant baculovirus, which allowed expression in SF9 cells (27).

Labeling of Calmodulin with Bifunctional Rhodamine. The bifunctional rhodamine used in the DOPI measurements was purchased from Invitrogen (part # B10621). The labeling or any other treatment of calmodulin was always on ice at approximately 4°C. The dye reacted with the calmodulin for 7 h on ice and then the mixture was dialyzed in 1 L buffer (See *SI Text* for buffer and further description) twice to remove any free dye. Samples were then flash frozen and stored at −20°C. To ensure that the dye properly attached via both linkers to a single calmodulin the mass spectrum of the labeled calmodulin was obtained. If the dye attached properly then the two iodines would be absent. If it did not label properly then one of the linker-iodines would be replaced by an OH- group.

Light-Chain Exchange. The labeled calmodulin was exchanged onto the IQ domain of the myosin VI HMM construct in 20 mM HEPES, pH 7.6, 25 mM KCl, 2 mM $MgCl_2$, 5 mM DTT, 1 mM EGTA, and 50 μM ATP. The concentration of myosin VI HMM in the buffer was 2 μM and the concentration of labeled calmodulin was 8 μM (a ratio of four calmodulins per myosin VI HMM). To remove the native unlabeled calmodulin, 1.2 mM $CaCl_2$ was added to the solution containing myosin VI and labeled calmodulin. The excess of Ca^{2+} caused the unlabeled calmodulin to be removed and a labeled calmodulin would be favored in binding to the open spot. After 10 min, 5 mM EGTA was added to chelate the free Ca^{2+} and stop the reaction. The sample was then run through a Sephadex G-75 spin column to remove unbound calmodulin. See *SI Text* for discussion on a second protocol for light-chain exchange.

Actin Immobilization and Myosin VI Motility. The actin was attached to the surface via biotin-streptavidin linker system. Actin was polymerized with a mixture of monomers with and without biotin such that approximately every tenth monomer in the filament was labeled with biotin. To attach the actin to the surface of a lab built flow cell, 1 mg/mL BSA-labeled biotin was flowed through the chamber followed by rinsing and 0.5 mg/mL streptavidin followed by another rinse. After BSA-streptavidin was attached, approximately 0.2 μM of polymerized actin was added. After rinsing the flow cell yet again, myosin VI was added to the flow cell and briefly imaged to ensure that it bound to the actin. For motility, the following buffer was added to the flow cell, 20 mM HEPES, pH 7.6, 25 mM KCl, 1 mM $MgCl_2$, 1 mM EGTA, 10 mM DTT, 10 μM ATP, and 0.05 mg/mL calmodulin, and our oxygen-scavenging system (11). It was found through trial and error that 10 μM allowed for individual steps to be resolved.

Imaging. A 532-nm diode pumped ND:YAG laser from CrystalLaser was used to excite the bifunctional rhodamine. Imaging was with an inverted Olympus microscope with a 100× NA 1.45 objective. Imaging was with a 512 × 512 pixels, 16 × 16 μM pixel size CCD camera from Andor. The dual view was purchased from Optical Insights.

ACKNOWLEDGMENTS. This work was supported by National Institutes of Health Grants GM068625 and GM072033 (to P.R.S.) and DC-009100 (to H.L.S.).

1. Wells AL, et al. (1999) Myosin VI is an actin-based motor that moves backwards. *Nature* 401:505–508.
2. Rock RS, et al. (2001) Myosin VI is a processive motor with a large step size. *Proc Natl Acad Sci USA* 98:13655–13659.
3. Ali MY, et al. (2004) Unconstrained steps of myosin VI appear longest among known molecular motors. *Biophys J* 86:3804–3810.
4. Chevreux G, et al. (2005) Electrospray ionization mass spectrometry studies of noncovalent myosin VI complexes reveal a new specific calmodulin binding site. *J Am Soc Mass Spectrom* 16:1367–1376.
5. Mukherjea M, et al. (2009) Myosin VI dimerization triggers an unfolding of a three-helix bundle in order to extend its reach. *Mol Cell* 35:305–315.
6. Okten Z, Churchman LS, Rock RS, Spudich JA (2004) Myosin VI walks hand-over-hand along actin. *Nat Struct Mol Biol* 11:884–887.
7. Yildiz A, et al. (2004) Myosin VI steps via a hand-over-hand mechanism with its lever arm undergoing fluctuations when attached to actin. *J Biol Chem* 279:37223–37226.
8. Sun Y, et al. (2007) Myosin VI walks ''wiggly'' on actin with large and variable tilting. *Mol Cell* 28:954–964.
9. Vale RD (2003) Myosin V motor proteins: Marching stepwise towards a mechanism. *J Cell Biol* 163:445–450.
10. Mehta AD, et al. (1999) Myosin V is a processive actin-based motor. *Nature* 400:590–593.
11. Yildiz A, et al. (2003) Myosin V walks hand-over-hand: Single fluorophore imaging with 1.5-nm localization. *Science* 300:2061–2065.
12. Forkey JN, Quinlan ME, Shaw MA, Corrie JE, Goldman YE (2003) Three-dimensional structural dynamics of myosin V by single-molecule fluorescence polarization. *Nature* 422:399–404.
13. Toprak E, et al. (2006) Defocused orientation and position imaging (DOPI) of myosin V. *Proc Natl Acad Sci USA* 103:6495–6499.
14. Syed S, Snyder GE, Franzini-Armstrong C, Selvin PR, Goldman YE (2006) Adaptability of myosin V studied by simultaneous detection of position and orientation. *EMBO J* 25:1795–1803.
15. Ali MY, et al. (2002) Myosin V is a left-handed spiral motor on the right-handed actin helix. *Nat Struct Biol* 9:464–467.
16. Ménétrey J, et al. (2005) The structure of the myosin VI motor reveals the mechanism of directionality reversal. *Nature* 435:779–785.
17. Ménétrey J, Llinas P, Mukherjea M, Sweeney HL, Houdusse A (2007) The structural basis for the large powerstroke of myosin VI. *Cell* 131:300–308.
18. Sweeney H L, et al. (2007) How myosin VI coordinates its heads during processive movement. *EMBO J* 26:2682–2692.
19. Park H, et al. (2007) The unique insert at the end of the myosin VI motor is the sole determinant of directionality. *Proc Natl Acad Sci USA* 104:778–783.
20. Bryant Z, Altman D, Spudich JA (2007) The power stroke of myosin VI and the basis of reverse directionality. *Proc Natl Acad Sci USA* 104:772–777.
21. Rosenfeld SS, Sweeney HL (2004) A model of myosin V processivity. *J Biol Chem* 279:40100–40111.
22. Altman D, Sweeney HL, Spudich JA (2004) The mechanism of myosin VI translocation and its load-induced anchoring. *Cell* 116:737–749.
23. Sweeney HL, Houdusse A (2007) What can myosin VI do in cells? *Curr Opin Cell Biol* 19:57–66.
24. Rock RS, et al. (2005) A flexible domain is essential for the large step size and processivity of myosin VI. *Mol Cell* 17:603–609.
25. Spink BJ, Sivaramakrishnan S, Lipfert J, Doniach S, Spudich JA (2008) Long single alpha-helical tail domains bridge the gap between structure and function of myosin VI. *Nat Struct Mol Biol* 15:591–597.
26. Yildiz A, et al. (2004) Myosin VI steps via a hand-over-hand mechanism with its lever arm undergoing fluctuations when attached to actin. *J Biol Chem* 279:37223–37226.
27. De La Cruz EM, Ostap EM, Sweeney HL (2001) Kinetic mechanism and regulation of myosin VI. *J Biol Chem* 276:32373–32381.